


Nonautonomous multi-peak solitons and modulation instability for a variable-coefficient nonlinear Schrödinger equation with higher-order effects

Liu-Ying Cai · Xin Wang · Lei Wang  ·
Min Li · Yong Liu · Yu-Ying Shi

Received: 19 May 2017 / Accepted: 7 September 2017 / Published online: 16 September 2017
© Springer Science+Business Media B.V. 2017

Abstract In this paper, we study a variable-coefficient nonlinear Schrödinger (vc-NLS) equation with fourth-order effects describing an inhomogeneous one-dimensional continuum anisotropic Heisenberg ferromagnetic spin chain or alpha helical protein. The first-order nonautonomous breather solution of the fourth-order vc-NLS equation is derived. The state transition between nonautonomous breather and nonautonomous multi-peak soliton can be realized when group velocity dispersion (GVD) coefficient is proportional to the fourth-order dispersion (FOD) coefficient. We also display how the higher-order effects influence the nonautonomous multi-peak solitons. Our results show that the velocity and localization of the nonautonomous multi-peak soliton are affected by the FOD coefficient, and the peak number is controlled by the GVD coefficient. Further, we also show the compression effect and motion

with variable velocity of nonautonomous multi-peak soliton in two kinds of dispersion management systems. Finally, we reveal the relation between the state transition and the modulation instability (MI) analysis.

Keywords Variable-coefficient nonlinear Schrödinger equation · Nonautonomous multi-peak soliton · Higher-order effects · Modulation instability

1 Introduction

There are two types of breathers, i.e., the Kuznetsov–Ma breathers (KMBs) [1,2] and Akhmediev breathers (ABs) [3,4]. The ABs are periodic in space and localized in time. On the contrary, the KMBs are periodic in time and localized in space. Taking the limit of these two solutions, we obtain the Peregrine soliton (PS) solution [5], which is regarded as a prototypical rogue wave (RW) profile in a series of experimental fields [6–8]. RWs, which are originally used to explain the extreme wave events in deep oceans [9], have recently been the subject of investigations in a wide range of complex nonlinear models with different mechanisms and physical backgrounds [10–16]. It appears from nowhere and disappears without a trace [17]. RW has a peak amplitude generally more than twice the significant wave height. In various models for describing RWs, the nonlinear Schrödinger (NLS) equation with the rational solution is considered to be the most accepted one. However, it has some restrictions in many physical backgrounds.

Liu-Ying Cai and Lei Wang are co-first authors.

L.-Y. Cai · L. Wang (✉) · M. Li · Y. Liu · Y.-Y. Shi
Department of Mathematics and Physics, North China
Electric Power University, Beijing 102206, People's
Republic of China
e-mail: 50901924@ncepu.edu.cn

Xin Wang
College of Science, Zhongyuan University of Technology,
Zhengzhou 450007,
People's Republic of China

Xin Wang
School of Mathematics and Statistics, Zhengzhou
University, 100 Kexue Road, Zhengzhou 450001, Henan,
People's Republic of China

Various factors such as the variation in the lattice parameters of the fiber medium and variation of the fiber geometry lead to some nonuniformities in the fiber. Therefore, the effects including the fiber gain or loss, self-phase modulation (SPM) and variable dispersion are produced [18]. In order to describe the effects of nonlinear effects on the propagation of optical pulses, we often consider the variable-coefficient nonlinear Schrödinger (vc-NLS) equation and other types of variable-coefficient models [19,20]. Such models, which offer more realistic description than their constant coefficient counterpart [21–26], have obtained extensive attention owing to the potential applications in dispersion management [27] and pulse compression [28]. Moreover, recent publications have shown that the RWs in nonautonomous systems provide certain novel characteristics such as the nonlinear tunneling effect, recurrence, annihilation and sustainment [29–32], to name a few. Besides, the studies of the control and manipulation of the RWs in the vc-NLS equations are useful to manage them experimentally in inhomogeneous optical fibers [32,33].

It is well known that the standard NLS equation can be used to describe the propagation of a picosecond optical pulse. However, the higher-order effects such as the third-order dispersion (TOD), higher-order nonlinearities and self-steepening (SS) are indispensable for describing the propagation of ultrashort pulses [34–39]. These effects may contribute to certain novel properties for the wave propagation behaviors [36,40,41]. Compared with the standard NLS equation, the higher-order NLS ones characterize the nonlinear wave phenomena more accurately in reality [36,37]. Additionally, a series of studies have shown that the higher-order effects account for the state transition between the breathers (or RWs) and other nonlinear waves on a continuous wave background [37,42–49]. These transitions do not exist in the standard NLS equation. For instance, Akhmediev et al. have indicated that a breather solution can be converted into a soliton one in the third- and fifth-order equations [50,51]. Wang et al. have discovered that the breathers can be transformed into various nonlinear waves in the fourth-order NLS equation [44]. Moreover, such state transitions have also been found in some higher-order coupled systems, i.e., the Hirota–Maxwell–Bloch (HMB) system [42], NLS-MB system [43] and coupled Hirota equation [47].

Currently, it is the most acceptable concept that the RW appears as a result of MI [52]. Interestingly, with certain higher-order perturbation terms such as the TOD and delayed nonlinear response term, the MI growth rate shows a non-uniform distribution characteristic in the low perturbation frequency region. In particular, it opens up a stability region as the background frequency changes [37,47]. In addition, using the RW eigenvalue, one can find that the modulation stability (MS) condition is consistent with the state transition condition, which converts RWs into solitons on constant backgrounds [44–46].

In this paper, we study the vc-NLS equation with the fourth-order [53–56],

$$\begin{aligned} iu_t + \alpha(t)u_{xx} + \beta(t)u|u|^2 \\ + \gamma_1(t)u_{xxxx} + \gamma_2(t)|u|^2u_{xx} \\ + \gamma_3(t)u^2u_{xx}^* + \gamma_4(t)u^*u_x^2 \\ + \gamma_5(t)|u_x|^2u + \gamma_6(t)|u|^4 = 0, \end{aligned} \quad (1.1)$$

where x is the propagation variable, t is the transverse variable, $u(x, t)$ represents the coherent amplitude in Glauber's coherent-state representation for the Heisenberg ferromagnetic spin chain or the probability amplitude of the excitation in the protein molecular chain [53], $\alpha(t)$, $\beta(t)$, $\gamma_i(t)$ ($i = 1, 2, \dots, 6$) are all the real functions of t . Equation (1.1) can be used to describe an inhomogeneous one-dimensional continuum anisotropic Heisenberg ferromagnetic spin chain or alpha helical protein [53–55]. In order to ensure the integrability of Eq. (1.1), all of these functions satisfy the linear relations, i.e., $\gamma_2(t) = 4\kappa\gamma_1(t)$, $\gamma_3(t) = \kappa\gamma_1(t)$, $\gamma_4(t) = 3\kappa\gamma_1(t)$, $\gamma_5(t) = 2\kappa\gamma_1(t)$, $\gamma_6(t) = \frac{3}{2}\kappa\gamma_1(t)$, $\beta(t) = \kappa\alpha(t)$. The coefficients $\alpha(t)$ and $\gamma_1(t)$ describe the GVD and FOD effects, respectively. The terms proportional to $\alpha(t)$ and $\gamma_1(t)$ represent the elementary spin excitations related to the lowest order of continuum approximation and octupole-dipole interaction, respectively [53]. Yang et al. have discussed the dynamics of soliton solution for Eq. (1.1) via the bilinear method [53]. They have shown the interactions between a bound state and a single soliton [53]. In addition, they have found that the RWs can be divided into many similar components when the variable coefficients are the polynomial functions, while the RWs can be divided into many different components when the variable coefficients are the hyperbolic secant functions [54]. Xie et al. have found that the directions of two solitons change and the elastic

interactions occur when the variable coefficients are functions [55]. Su et al. have reported the influences of the GVD, TOD, FOD and gain or loss coefficient on the propagation and interaction of the nonautonomous breathers and RWs for Eq. (1.1) [56]. To the best of our knowledge, the dynamics of nonautonomous multi-peak solitons and MI characteristic for Eq. (1.1) have not been reported in the existing papers, which are the main results of this paper.

The arrangement of this paper is as follows: In Sect. 2, we will discuss the dynamics of nonautonomous multi-peak soliton for Eq. (1.1). The state transition condition between nonautonomous breathers and nonautonomous multi-peak solitons will be given. Further, the characteristics of multi-peak solitons will be studied. The relation between the MI and state transition condition will be revealed in Sect. 3. Finally, Sect. 4 will give the conclusions of this paper.

2 The dynamics of the nonautonomous multi-peak soliton

In this section, by using the Darboux transformation (DT), the expression of the first-order nonautonomous breather solution of Eq. (1.1) can be given by

$$q_B^{[1]} = \left(c + 8\beta_1 \frac{G_B^{[1]} + i H_B^{[1]}}{D_B^{[1]}} \right) e^{i\rho}, \tag{2.1}$$

with

$$\begin{aligned} \rho &= rx + s(t), \\ s(t) &= \int \left((-r^2 + c^2\kappa)\alpha(t) + \frac{1}{2}(2r^4 - 12r^2c^2\kappa + 3c^4\kappa^2)\gamma_1(t) \right) dt, \\ G_B^{[1]} &= k_1 k_2 \chi_1 \cos(t V_H + x \omega_R) \\ &\quad + c(2 + \kappa) M \cosh(t V_T + x \omega_I) \\ &\quad + c(-2 + \kappa) M \sinh(t V_T + x \omega_I), \\ H_B^{[1]} &= c(-2 + \kappa) N \cosh(t V_T + x \omega_I) \\ &\quad + k_1 k_2 \chi_2 \sin(t V_H + x \omega_R) \\ &\quad + c(2 + \kappa) N \sinh(t V_T + x \omega_I), \\ D_B^{[1]} &= 8\kappa c k_1 k_2 M \cos(t V_H + x \omega_R) \\ &\quad + (2 + \kappa) \chi_1 \cosh(t V_T + x \omega_I) \\ &\quad + (-2 + \kappa) \chi_1 \sinh(t V_T + x \omega_I), \\ \omega &= 2\sqrt{\frac{\kappa}{2}c^2 + \left(\frac{r}{2} + \lambda\right)^2} = (\omega_R + i\omega_I), \end{aligned}$$

$$\begin{aligned} h &= [x + (\alpha(t)(2\lambda - r) + \gamma_1(t)(r^3 - 2r^2\lambda + 2c^2\kappa\lambda - 8\lambda^3 - 3c^2\kappa r + 4\lambda^2r))t] \frac{\omega}{2} \\ &= [x + (h_R + ih_I)t] \frac{\omega}{2}, \\ \chi_1 &= r^2 + h_I^2 - 2r h_R + h_R^2 + 4r\alpha_1 - 4h_R\alpha_1 \\ &\quad + 4\alpha_1^2 - 4h_I\beta_1 + 4\beta_1^2 + 2c^2\kappa, \\ \chi_2 &= r^2 + h_I^2 - 2r h_R + h_R^2 + 4r\alpha_1 - 4h_R\alpha_1 \\ &\quad + 4\alpha_1^2 - 4h_I\beta_1 + 4\beta_1^2 - 2c^2\kappa, \\ k_1 &= 1, \quad k_2 = -1, \\ M &= h_I - 2\beta_1, \quad N = r - h_R + 2\alpha_1, \\ V_T &= 2(h_R\omega_I + h_I\omega_R), \\ V_H &= 2(h_R\omega_R - h_I\omega_I). \end{aligned}$$

We note that Eq. (2.1) contains two variable coefficients, i.e., the GVD coefficient $\alpha(t)$ and FOD coefficient $\gamma_1(t)$, which can be flexibly manipulated according to different physical backgrounds. For example, Fig. 1 displays the periodic accelerating and decelerating motions of the first-order nonautonomous breather with $\alpha(t) = 1, \gamma_1(t) = \cos(t)$. Further, from Eq. (2.1), we can calculate two significant physical quantities, namely the phase velocity $V_p = h_R + \frac{h_I\omega_R}{\omega_I}$ and group velocity $V_g = h_R - \frac{h_I\omega_I}{\omega_R}$. Generally speaking, Eq. (2.1) describes the dynamics of nonautonomous breather when $V_p \neq V_g$ (or $h_I \neq 0$). In this case, the expression (2.1) contains both hyperbolic functions and trigonometric functions. However, if the phase velocity and group velocity have same value, i.e., $V_p = V_g$ (or $h_I = 0$), the state transition between nonautonomous breather and nonautonomous multi-peak soliton can be achieved. From Eq. (2.1), one can find that the phase velocity and group velocity can be controlled by initial wave number r . Therefore, we can get some special values of r by solving $V_p = V_g$. Figure 2 describes the locus of V_p and V_g . When $r = 2.32337$ and $r = -1.12337$, we have $V_p = V_g$, shown by the wine red dots in Fig. 2. Additionally, it should be pointed out that the case $V_p = V_g$ is equivalent to

$$\frac{V_T}{\omega_I} = \frac{V_H}{\omega_R}, \tag{2.2}$$

i.e.,

$$\frac{\alpha(t)}{\gamma_1(t)} = \frac{1}{r^2 - 4r\alpha_1 + 12\alpha_1^2 - 4\beta_1^2 - c^2\kappa}. \tag{2.3}$$

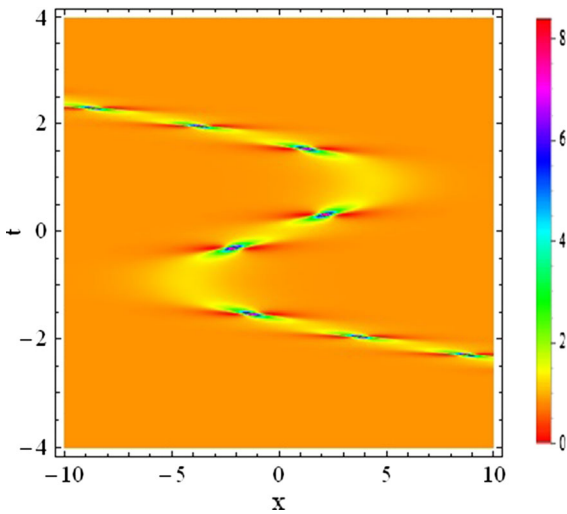


Fig. 1 First-order nonautonomous breather with $r = 0.3$, $c = 0.9$, $\gamma_1(t) = \cos(t)$, $\alpha(t) = 1$, $\alpha_1 = -0.15$, $\beta_1 = 1$, $\kappa = 2$

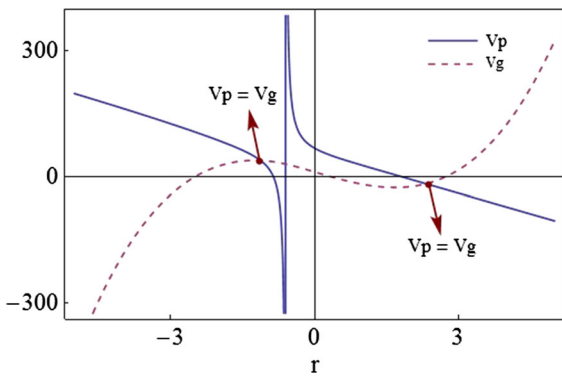


Fig. 2 Locus of phase velocity and group velocity with $c = 1$, $\gamma_1(t) = 4$, $\alpha(t) = 1$, $\alpha_1 = 0.3$, $\beta_1 = -0.6$, $\kappa = 2$

Equation. (2.2) [or Eq. (2.3)] implies the extrema of trigonometric and hyperbolic functions in the solution Eq. (2.1) is located along the same straight lines in the (x, t) plane, which leads to the transformation of the breather into a continuous soliton. Moreover, we should point out that GVD and FOD coefficients need to meet a directly proportional relationship to achieve the state transition. Otherwise, Eq. (2.3) has no solution with respect to r . This is different from the constant coefficient case in Ref. [44].

In order to exhibit the dynamical properties of Eq. (1.1), we discuss the effects of the FOD coefficient $\gamma_1(t)$ and GVD coefficient $\alpha(t)$ on the nonautonomous multi-peak soliton.

Firstly, we consider the effects of higher-order terms on the velocity of the multi-peak soliton. From Eq. (2.1), we can see that the group velocity contains the FOD coefficient. Selecting two different values of $\gamma_1(t)$ [$\gamma_1(t) = 0.58$ and $\gamma_1(t) = 0.32$] will lead to different values of the group velocity V_g . As shown in Fig. 3a, b, the nonautonomous multi-peak soliton have negative velocity ($h_R < 0$) and positive velocity ($h_R > 0$), respectively. In other words, the higher-order terms have the effect on the direction of the nonautonomous multi-peak soliton. Additionally, the similar influence of higher-order effects on the velocity of other nonlinear structures such as the standard solitons, breathers and RWs, have also been found in different higher-order NLS models [57–59].

Secondly, we study the effects of higher-order terms on the localization of the multi-peak soliton. Fixing the value of $\alpha(t)$, we change the value of $\gamma_1(t)$. By choosing $\gamma_1(t) = 0.029$ and $\gamma_1(t) = 0.089$, Fig. 4a, b, respectively, shows a strong localization and a weak localization of the multi-peak solitons along the x -direction. This reflects the second significant effect of the FOD term on the multi-peak soliton, in addition to the velocity. However, the effects of FOD term have no obvious effects on the peak number and amplitude of the multi-peak soliton. In particular, the localization of the wave vanishes completely with $\gamma_1(t) = 0.298$. In this case, the multi-peak soliton is transformed into a periodic wave with vanishing localization, which is displayed in Fig. 4c. Correspondingly, the exact expression of the periodic wave reads as

$$q_p^{[1]} = \left(c + 8\beta_1 \frac{G_p^{[1]} + i H_p^{[1]}}{D_p^{[1]}} \right) e^{i\rho}, \tag{2.4}$$

with

$$\begin{aligned} G_p^{[1]} &= k_1 k_2 \chi_{11} \cos(\omega_R(x + 2t h_R)) + c(2 + \kappa) M_1, \\ H_p^{[1]} &= c(-2 + \kappa) N_1 + k_1 k_2 \chi_{12} \sin(\omega_R(x + 2t h_R)), \\ D_p^{[1]} &= 8\kappa c k_1 k_2 M_1 \cos(\omega_R(x + 2t h_R)) + (2 + \kappa) \chi_{11}, \\ \chi_{11} &= r^2 - 2r h_R + h_R^2 + 4r \alpha_1 - 4h_R \alpha_1 + 4\alpha_1^2 \\ &\quad + 4\beta_1^2 + 2c^2 \kappa, \\ \chi_{12} &= r^2 - 2r h_R + h_R^2 + 4r \alpha_1 - 4h_R \alpha_1 + 4\alpha_1^2 \\ &\quad + 4\beta_1^2 - 2c^2 \kappa, \\ M_1 &= -2\beta_1, \quad N_1 = r - h_R + 2\alpha_1. \end{aligned}$$

Thirdly, we investigate the effects of GVD term on the multi-peak soliton. Unlike the previous discussions,

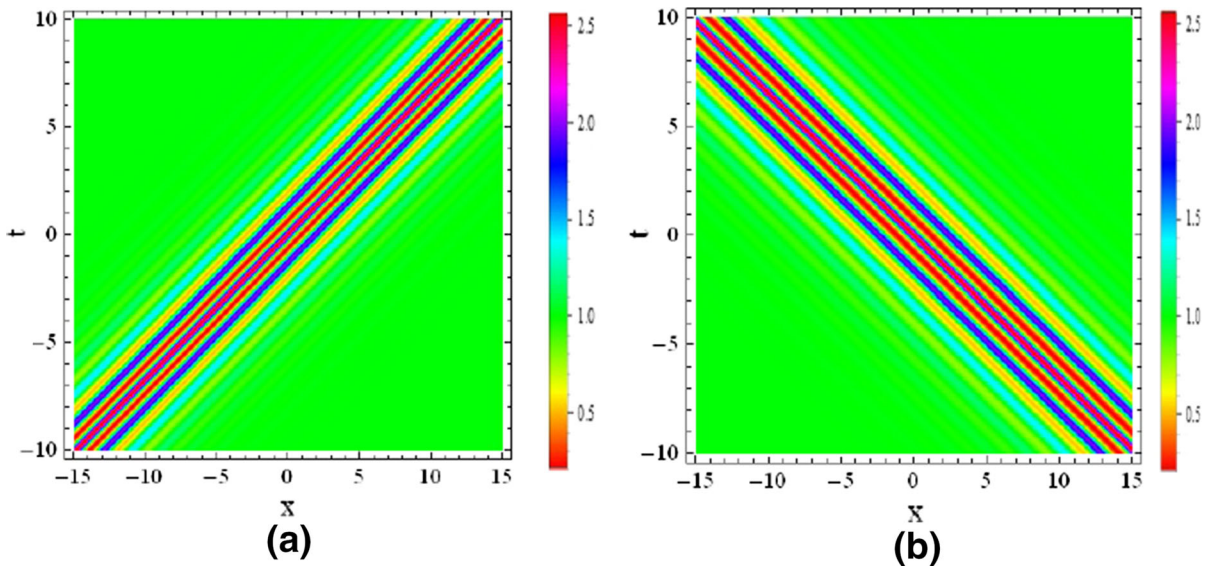


Fig. 3 Effects of FOD term on the velocity of nonautonomous multi-peak soliton with $\gamma_1(t)$, **a** $\gamma_1(t) = 0.58$, **b** $\gamma_1(t) = 0.32$. Other parameters are $c = 1, \alpha_1 = 0.7, \beta_1 = -0.3, \alpha(t) = 1, \kappa = 2$

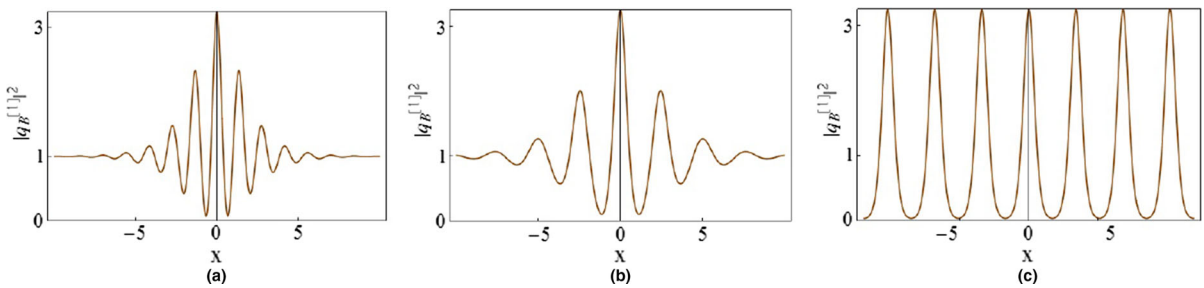


Fig. 4 Effects of FOD term on the localization of nonautonomous multi-peak solitons with $\gamma_1(t)$, **a** $\gamma_1(t) = 0.029$, **b** $\gamma_1(t) = 0.089$, **c** $\gamma_1(t) = 0.298$. Other parameters are $c = 1, \alpha_1 = 0.5, \beta_1 = -0.4, \alpha(t) = 1, \kappa = 2$

we adjust the value of $\alpha(t)$ while fixing the value of $\alpha(t)$. As depicted in Fig. 5, we find that increasing the values of $\alpha(t)$ leads to a stronger localization and a smaller oscillation period for the multi-peak soliton. Moreover, the GVD coefficient $\alpha(t)$ can change the number of peaks of the soliton. We observe that the wave described by the dashed purple curve [$\alpha(t) = 3.47$] has nine humps, while the wave described by the solid blue curve [$\alpha(t) = 4.45$] has fifteen humps. In other words, as the value of $\alpha(t)$ increases, the number of peaks of soliton increases. However, the amplitude of the main peak remains unchangeable. This suggests that the GVD coefficient $\alpha(t)$ not only affects the localization of the soliton, but also controls its peak number.

Fourthly, we consider an exponential fiber system, letting $\gamma_1(t)$ and $\alpha(t)$ as two linearly related functions.

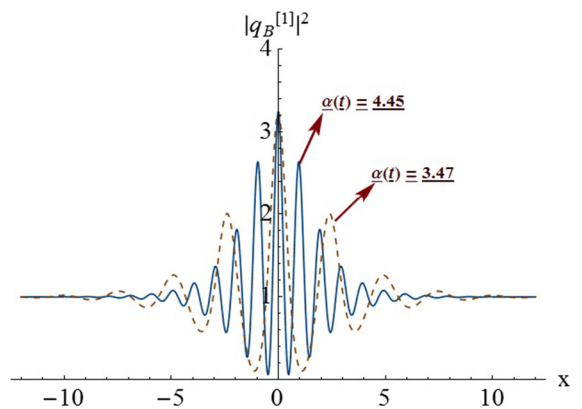


Fig. 5 Effects of GVD term on the peak number of nonautonomous multi-peak solitons with $\gamma_1(t) = 0.29, c = 1, \alpha_1 = 0.5, \beta_1 = -0.4, \kappa = 2$

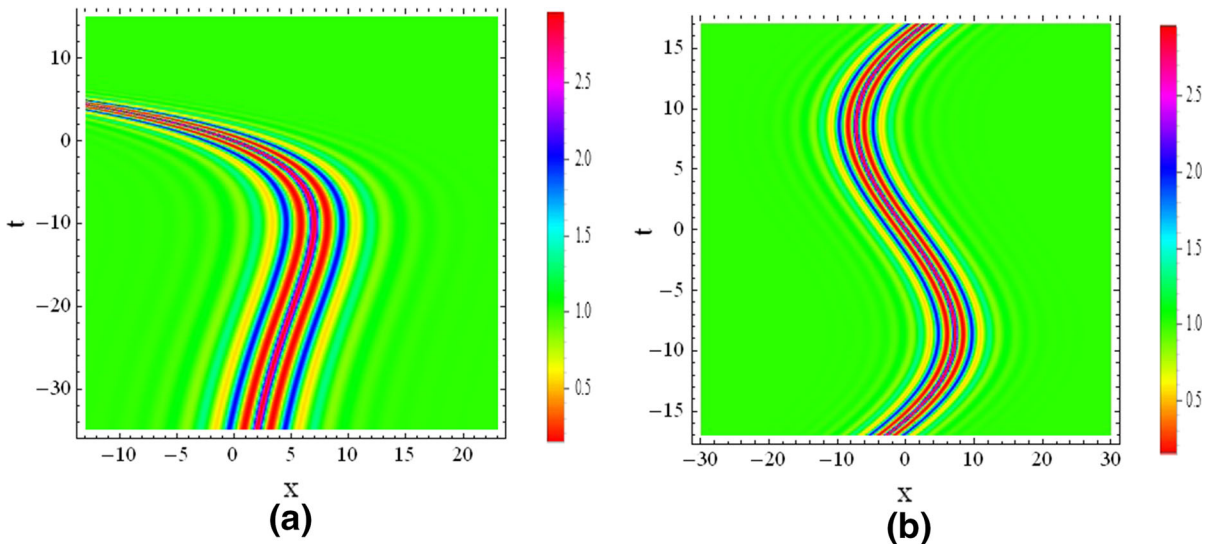


Fig. 6 **a** Compression effect of nonautonomous multi-peak solitons with $r = 0.5, c = 1, \sigma_1 = -4.328, \sigma_2 = 1, \alpha_1 = 0.504, \beta_1 = -0.36, \kappa = 2, \varepsilon = 0.1$. **b** Periodic variable motion of

multi-peak solitons with $r = 0.5, c = 1, \sigma_1 = -2.157, \sigma_2 = 1, \alpha_1 = 0.48, \beta_1 = -0.36, \kappa = 2, \varepsilon = 0.1$

For instance,

$$\gamma_1(t) = \sigma_1 \exp(\varepsilon t), \quad \alpha(t) = \sigma_2 \exp(\varepsilon t). \quad (2.5)$$

where the variable parameters σ_1 and σ_2 are connected with the FOD and GVD effects, the parameter ε is a constant. In Fig. 6a, we observe that the velocity and width of the multi-peak soliton change during the propagation. The case $\varepsilon < 0$ causes the multi-peak soliton to be compressed, whereas $\varepsilon > 0$ results in the multi-peak soliton to be amplified.

Finally, we consider a soliton management system, which is similar to that of Ref. [60], i.e., the periodic distributed system

$$\gamma_1(t) = \sigma_1 \cos(\varepsilon t), \quad \alpha(t) = \sigma_2 \cos(\varepsilon t). \quad (2.6)$$

where trigonometric functions are physically relevant because they provide opposite (positive and negative) dispersion and nonlinearity with alternating regions. As shown in Fig. 6b, the multi-peak soliton is periodic acceleration and deceleration in the propagation.

From the above analysis, we can find that when the GVD coefficient $\alpha(t)$ and FOD coefficient $\gamma_1(t)$ satisfy the condition (2.3), the nonautonomous breather can be transformed into nonautonomous multi-peak

soliton in a one-dimensional continuum anisotropic Heisenberg ferromagnetic spin chain or alpha helical protein. In addition, we find that the lowest order of continuum approximation and octupole–dipole interaction in a Heisenberg ferromagnetic spin chain do not influence the amplitude of the soliton, but they influence the velocity, localization and peak number of the nonautonomous multi-peak soliton, respectively. For the detailed discussions of relation between the interactions between/among the two and three solitons and the ferromagnetism, one can refer to [53,61].

3 MI characteristics

In this section, we reveal the explicit relation between the state transition and MI characteristic for Eq. (1.1) by linear stability analysis. The plane-wave solution of Eq. (1.1) is presented as

$$u(x, t) = c e^{i(r x + s(t))}, \quad (3.1)$$

where c and r are two real parameters. The perturbation solution can be expressed as

$$u(x, t) = (c + \varepsilon \hat{u}(x, t)) e^{i(r x + s(t))}, \quad (3.2)$$

where $\hat{u}(x, t)$ is the small-amplitude perturbation [62]. Substituting Eq. (3.2) into Eq. (1.1) yields the evolution equation for the perturbation $\hat{u}(x, t)$ as

$$\begin{aligned}
 &\kappa c^2 \alpha(t) \widehat{u}(x, t) - 6\kappa r^2 c^2 \gamma_1(t) \widehat{u}(x, t) \\
 &+ 3\kappa^2 c^4 \gamma_1(t) \widehat{u}(x, t) \\
 &+ \kappa c^2 \alpha(t) \widehat{u}^*(x, t) - 6\kappa c^2 r^2 \gamma_1(t) \widehat{u}^*(x, t) \\
 &+ 3\kappa^2 c^4 \gamma_1(t) \widehat{u}^*(x, t) \\
 &+ i \widehat{u}^{(0,1)}(x, t) + 2i r \alpha(t) \widehat{u}^{(1,0)}(x, t) \\
 &- 4i r^3 \gamma_1(t) \widehat{u}^{(1,0)}(x, t) \\
 &+ 12\kappa i r c^2 \gamma_1(t) \widehat{u}^{(1,0)}(x, t) + \alpha(t) \widehat{u}^{(2,0)}(x, t) \\
 &- 6r^2 \gamma_1(t) \widehat{u}^{(2,0)}(x, t) + 4\kappa c^2 \gamma_1(t) \widehat{u}^{(2,0)}(x, t) \\
 &+ \kappa c^2 \gamma_1(t) \widehat{u}^{*(2,0)}(x, t) + 4i r \gamma_1(t) \widehat{u}^{(3,0)}(x, t) \\
 &+ \gamma_1(t) \widehat{u}^{(4,0)}(x, t) = 0. \tag{3.3}
 \end{aligned}$$

Noting that the linearity of Eq. (3.3) with respect to $\widehat{u}(x, t)$, we introduce

$$\widehat{u}(x, t) = \text{U1} e^{i(Qx - \varpi(t))} + \text{V1} e^{-i(Qx - \varpi^*(t))}, \tag{3.4}$$

which is characterized by the frequency $\varpi(t)$ and wave number Q . Using Eq. (3.4) into Eq. (3.3) gives a linear homogeneous system of equations for U1 and V1:

$$\begin{aligned}
 &- 2r Q \text{U1} \alpha(t) - Q^2 \text{U1} \alpha(t) + \kappa c^2 \text{U1} \alpha(t) \\
 &+ \kappa c^2 \text{V1} \alpha(t) + 4r^3 Q \text{U1} \gamma_1(t) + 6r^2 Q^2 \text{U1} \gamma_1(t) \\
 &- 6\kappa r^2 c^2 \text{U1} \gamma_1(t) - 12\kappa r c^2 Q \text{U1} \gamma_1(t) \\
 &- 4\kappa c^2 Q^2 \text{U1} \gamma_1(t) - 6\kappa r^2 c^2 \text{V1} \gamma_1(t) \\
 &- \kappa c^2 Q^2 \text{V1} \gamma_1(t) + 3\kappa^2 c^4 \text{U1} \gamma_1(t) \\
 &+ 3\kappa^2 c^4 \text{V1} \gamma_1(t) + \text{U1} \varpi'(t) = 0, \tag{3.5}
 \end{aligned}$$

$$\begin{aligned}
 &2r Q \text{V1} \alpha(t) - Q^2 \text{V1} \alpha(t) + \kappa c^2 \text{U1} \alpha(t) \\
 &+ \kappa c^2 \text{V1} \alpha(t) - 4r^3 Q \text{V1} \gamma_1(t) + 6r^2 Q^2 \text{V1} \gamma_1(t) \\
 &- 6\kappa r^2 c^2 \text{V1} \gamma_1(t) + 12\kappa r c^2 Q \text{V1} \gamma_1(t) \\
 &- 4\kappa c^2 Q^2 \text{V1} \gamma_1(t) - 6\kappa r^2 c^2 \text{U1} \gamma_1(t) \\
 &- \kappa c^2 Q^2 \text{U1} \gamma_1(t) + 3\kappa^2 c^4 \text{U1} \gamma_1(t) \\
 &+ 3\kappa^2 c^4 \text{V1} \gamma_1(t) - \text{V1} \varpi'(t) = 0. \tag{3.6}
 \end{aligned}$$

From the determinant of the coefficient matrix of Eqs. (3.5)–(3.6), the dispersion relation for the linearized disturbance can be determined as

$$\varpi^2(t) + J_1 \varpi(t) + J_0 = 0, \tag{3.7}$$

with

$$\begin{aligned}
 J_1 &= -4r Q (4r^2 \gamma_1(t) + 3\kappa c^2 \gamma_1(t) + Z), \\
 J_0 &= Q^2(\alpha(t)^2(4r^2 - Q^2 + 2\kappa c^2) \\
 &+ 4(-4r^4 + \kappa c^2(-2Q^2 + 3\kappa c^2))\alpha(t)\gamma_1(t)
 \end{aligned}$$

$$\begin{aligned}
 &+ (16r^6 - 12r^4(3Q^2 + 2\kappa c^2) \\
 &+ 24\kappa r^2 c^2(2Q^2 + 3\kappa c^2) \\
 &+ 3\kappa^2 c^4(-5Q^2 + 6\kappa c^2))\gamma_1(t)^2), \\
 Z &= \alpha(t) - 6r^2 \gamma_1(t) + 3\kappa c^2 \gamma_1(t).
 \end{aligned}$$

Solving the above equation, we have

$$\begin{aligned}
 \varpi(t) &= 2r Q(4r^2 \gamma_1(t) + 3\kappa c^2 \gamma_1(t) + Z) \\
 &\pm Q \sqrt{Z(Q^2(2\kappa c^2 \gamma_1(t) + Z) - 2\kappa Z c^2)}, \tag{3.8}
 \end{aligned}$$

In this case, the frequency $\varpi(t)$ becomes complex and the disturbance will grow with time exponentially if and only if $Q^2 < Q_c^2 = \frac{2\kappa Z c^2}{2\kappa c^2 \gamma_1(t) + Z}$, and the growth rate of the instability is given by

$$\Gamma = |Q| \sqrt{Z(-Q^2(2\kappa c^2 \gamma_1(t) + Z) + 2\kappa Z c^2)}. \tag{3.9}$$

To obtain the maximum growth rate of the instability, we take the derivative of Eq. (3.9) with respect to Q , and set it to zero. Then, we obtain

$$Q_{\max} = \pm \sqrt{\frac{\kappa c^2 Z}{2\kappa c^2 \gamma_1(t) + Z}}, \tag{3.10}$$

and the following maximum growth rate of the instability:

$$\Gamma_{\max} = \frac{\kappa c^2 |Z|}{\sqrt{2\kappa c^2 \gamma_1(t)/Z + 1}}. \tag{3.11}$$

From Fig. 7, we can see that the distribution characteristic of MI gain is impacted by the FOD coefficient in the region $-\sqrt{2\kappa} c < Q < \sqrt{2\kappa} c$, and it has two symmetric modulation stability (MS) region where the MI growth rate is vanishing in the low perturbation frequency region. The MS regions are characterized by the two dashed orange lines in Fig. 7. Moreover, the expression of the MS regions is given by

$$r = r_s = \pm \sqrt{\frac{\alpha(t)}{6\gamma_1(t)} + \frac{\kappa c^2}{2}}, \tag{3.12}$$

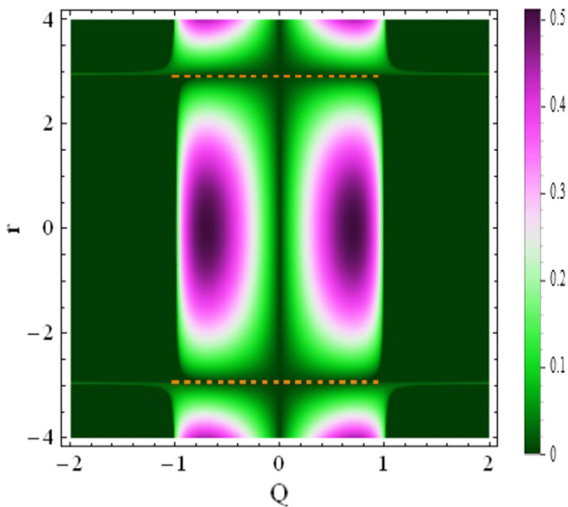


Fig. 7 Characteristics of MI growth rate ω on (Q, r) plane with $c=0.5, \kappa = 2, \alpha(t) = 1, \gamma_1(t) = 0.02$. Here the dashed orange lines represent the stability region in the perturbation frequency region $-\sqrt{2\kappa c} < Q < \sqrt{2\kappa c}$, which is presented as $r = r_s = \pm\sqrt{\frac{\alpha(t)}{6\gamma_1(t)} + \frac{\kappa c^2}{2}}$. (Color figure online)

i.e.,

$$\gamma_1(t) = \frac{\alpha(t)}{6r^2 - 3\kappa c^2}. \tag{3.13}$$

We note that the MS condition (3.13) requires a special coefficient relationship where $\gamma_1(t)$ is proportional to $\alpha(t)$. This is consistent with the soliton management system described by Eqs. (2.5) and (2.6). Further, using the RW eigenvalue $\lambda_0 = -\frac{r}{2} + i\frac{\sqrt{2\kappa}}{2}c$, we find the state transition (2.3) is consistent with the MS region condition (3.13). Our results show that the state transition between the RWs and multi-peak solitons can exist in the MS region with low frequency perturbation.

4 Conclusions

We have presented the first-order nonautonomous breather solution for Eq. (1.1) and the state transition between nonautonomous breather and nonautonomous multi-peak soliton. We have discussed the effects of higher-order terms on the nonautonomous multi-peak soliton, including the velocity, localization, peak number and width. We have also shown that the state transition condition is consistent with the MS region condition when the RW eigenvalue is taken.

Acknowledgements We express our sincere thanks to all the members of our discussion group for their valuable comments. This work has been supported by the National Natural Science Foundation of China under Grant (Nos. 11305060, 11271126, 11705290 and 61505054), by the Fundamental Research Funds of the Central Universities (Project No. 2015ZD16), by China Postdoctoral Science Foundation funded sixtieth batches (No. 2016M602252). Lei Wang put forward the idea of this paper. Lei Wang and Liu-ying Cai contributed all mathematical calculation and physical analysis. Lei Wang and Liu-ying Cai wrote the paper. Xin Wang, Min Li, Yong Liu and Yu-ying Shi polished the language. Liu-ying Cai generated all the figures and was responsible for all simulations.

References

1. Ma, Y.C.: The perturbed plane-wave solutions of the cubic Schrödinger equation. *Stud. Appl. Math.* **60**, 43 (1979)
2. Kibler, B., Fatome, J., Finot, C., Millot, G., Genty, G., Wetzel, B., Akhmediev, N., Dias, F., Dudley, J.M.: Observation of Kuznetsov–Ma soliton dynamics in optical fibre. *Sci. Rep.* **236**, 463 (2012)
3. Akhmediev, N.N., Kornee, V.I.: Modulation instability and periodic solutions of the nonlinear Schrödinger equation. *Theor. Math. Phys.* **69**, 1089 (1986)
4. Dudley, J.M., Dias, F., Erkintalo, M., Genty, G.: Instabilities, breathers and rogue waves in optics. *Nat. Photonics* **8**, 755 (2014)
5. Peregrine, D.H.: Water waves, nonlinear Schrödinger equations and their solutions. *J. Aust. Math. Soc. Ser. B* **25**, 16 (1983)
6. Shrira, V.I., Geogjaev, V.V.: What makes the Peregrine soliton so special as a prototype of freak waves? *J. Eng. Math.* **67**, 11 (2010)
7. Yang, G., Li, L., Jia, S., Mihalache, D.: High power pulses extracted from the Peregrine rogue wave. *Rom. Rep. Phys.* **65**, 391 (2013)
8. Onorato, M., Residori, S., Bortolozzo, U., Montina, A., Arecchi, F.T.: Rogue waves and their generating mechanisms in different physical contexts. *Phys. Rep.* **528**, 47 (2013)
9. Kharif, C., Pelinovsky, E.: Physical mechanisms of the rogue wave phenomenon. *Eur. J. Mech. B Fluids* **22**, 603 (2003)
10. Chabchoub, A., Hoffmann, N., Onorato, M., Akhmediev, N.: Super rogue waves: observation of a higher-order breather in water waves. *Phys. Rev. X* **106**, 011015 (2012)
11. Osborne, A.R.: *Nonlinear Ocean Waves and the Inverse Scattering Transform*. Elsevier, Amsterdam (2010)
12. Bailung, H., Sharma, S.K., Nakamura, Y.: Observation of Peregrine solitons in a multicomponent plasma with negative ions. *Phys. Rev. Lett.* **107**, 255005 (2011)
13. Porter, A., Smyth, N.F.: Modelling the morning glory of the Gulf of Carpentaria. *J. Fluid Mech.* **454**, 1 (2002)
14. Soto-Crespo, J.M., Grelu, P., Akhmediev, N.: Dissipative rogue waves: extreme pulses generated by passively mode-locked lasers. *Phys. Rev. E* **84**, 016604 (2011)
15. Dai, C.Q., Tian, Q., Zhu, S.Q.: Controllable optical rogue waves in the femtosecond regime. *Phys. Rev. E* **85**, 016603 (2012)

16. Wang, L., Jiang, D.Y., Qi, F.H., Shi, Y.Y., Zhao, Y.C.: Dynamics of the higher-order rogue waves for a generalized mixed nonlinear Schrödinger model. *Commun. Nonlinear Sci. Numer. Simul.* **42**, 502 (2017)
17. Akhmediev, N., Ankiewicz, A., Taki, M.: Waves that appear from nowhere and disappear without a trace. *Phys. Lett. A* **373**, 675 (2009)
18. Agrawal, G.P.: *Nonlinear Fiber Optics*, 3rd edn. Academic Press, San Diego (2002)
19. Li, M., Tian, B., Liu, W.J., Zhang, H.Q., Meng, X.H., Xu, T.: Soliton-like solutions of a derivative nonlinear Schrödinger equation with variable coefficients in inhomogeneous optical fibers. *Nonlinear Dyn.* **62**, 919 (2010)
20. Gao, X.Y.: Density-fluctuation symbolic computation on the (3+1)-dimensional variable-coefficient Kudryashov Sinelshchikov equation for a bubbly liquid with experimental support. *Mod. Phys. Lett. B* **30**, 1650217 (2016)
21. Gao, X.Y.: Bäcklund transformation and shock-wave-type solutions for a generalized (3+1)-dimensional variable-coefficient B-type Kadomtsev–Petviashvili equation in fluid mechanics. *Ocean Eng.* **96**, 245 (2015)
22. Wang, X., Liu, C., Wang, L.: Darboux transformation and rogue wave solutions for the variable-coefficients coupled Hirota equations. *J. Math. Anal. Appl.* **449**, 1534 (2017)
23. Lü, X., Peng, M.: Nonautonomous motion study on accelerated and decelerated solitons for the variable-coefficient Lenells–Fokas model. *Chaos* **23**, 013122 (2013)
24. Kruglov, V.I., Peacock, A.C., Harvey, J.D.: Exact self-similar solutions of the generalized nonlinear Schrödinger equation with distributed coefficients. *Phys. Rev. Lett.* **90**, 113902 (2003)
25. Wang, L., Li, X., Qi, F.H., Zhang, L.L.: Breather interactions and higher-order nonautonomous rogue waves for the inhomogeneous nonlinear Schrödinger Maxwell–Bloch equations. *Ann. Phys.* **359**, 97 (2015)
26. Wang, L., Zhu, Y.J., Qi, F.H., Li, M., Guo, R.: Modulational instability, higher-order localized wave structures, and nonlinear wave interactions for a nonautonomous Lenells–Fokas equation in inhomogeneous fibers. *Chaos* **25**, 063111 (2015)
27. Bogatyrev, V.A., Bubnov, M.M., Dianov, E.M., Kurkov, A.S., Mamyshev, P.V., Prokhorov, A.M., Romyantsev, S.D., Semenov, V.A., Semenov, S.L., Sysoliatin, A.A., Chernikov, S.V., Guryanov, A.N., Devyatkykh, G.G., Miroshnichenko, S.I.: A single-mode fiber with chromatic dispersion varying along the length. *J. Lightwave Technol.* **9**, 561 (1991)
28. Kruglov, V.I., Peacock, A.C., Harvey, J.D.: Exact solutions of the generalized nonlinear Schrödinger equation with distributed coefficients. *Phys. Rev. E* **71**, 056619 (2005)
29. Yan, Z.Y., Konotop, V.V., Akhmediev, N.: Three-dimensional rogue waves in nonstationary parabolic potentials. *Phys. Rev. E* **82**, 036610 (2010)
30. Zhong, W.P., Belić, M., Malomed, B.A., Huang, T.W.: Breather management in the derivative nonlinear Schrödinger equation with variable coefficients. *Ann. Phys.* **355**, 313 (2015)
31. He, J.S., Tao, Y.S., Porsezian, K., Fokas, A.S.: Rogue wave management in an inhomogeneous Nonlinear Fibre with higher order effects. *J. Nonlinear Math. Phys.* **20**, 407 (2013)
32. Dai, C.Q., Zhou, G.Q., Zhang, J.F.: Controllable optical rogue waves in the femtosecond regime. *Phys. Rev. E* **85**, 016603 (2012)
33. Zhong, W.P., Chen, L., Belić, M., Petrović, N.: Controllable parabolic-cylinder optical rogue wave. *Phys. Rev. E* **90**, 043201 (2014)
34. Gao, X.Y.: Looking at a nonlinear inhomogeneous optical fiber through the generalized higher-order variable-coefficient Hirota equation. *Appl. Math. Lett.* **73**, 143 (2017)
35. Liu, L., Tian, B., Chai, H.P., Yuan, Y.Q.: Certain bright soliton interactions of the Sasa–Satsuma equation in a monomode optical fiber. *Phys. Rev. E* **95**, 032202 (2017)
36. Liu, C., Yang, Z.Y., Zhao, L.C., Duan, L., Yang, G.Y., Yang, W.L.: Symmetric and asymmetric optical multipeak solitons on a continuous wave background in the femtosecond regime. *Phys. Rev. E* **94**, 042221 (2016)
37. Liu, C., Yang, Z.Y., Zhao, L.C., Yang, W.L.: State transition induced by higher-order effects and background frequency. *Phys. Rev. E* **91**, 022904 (2015)
38. Chai, J., Tian, B., Zhen, H.L., Sun, W.Y., Liu, D.Y.: Dynamic behaviors for a perturbed nonlinear Schrödinger equation with the power-law nonlinearity in a non-Kerr medium. *Commun. Nonlinear Sci. Numer. Simul.* **45**, 93 (2017)
39. Marklund, M., Shukla, P.K., Stenflo, L.: Ultrashort solitons and kinetic effects in nonlinear metamaterials. *Phys. Rev. E* **73**, 037601 (2006)
40. Wang, L., Wang, Z.Q., Sun, W.R., Shi, Y.Y., Li, M., Xu, M.: Dynamics of Peregrine combs and Peregrine walls in an inhomogeneous Hirota and Maxwell–Bloch system. *Commun. Nonlinear Sci. Numer. Simul.* **47**, 190 (2017)
41. Zhao, L.C., Li, S.C., Ling, L.M.: W-shaped solitons generated from a weak modulation in the Sasa–Satsuma equation. *Phys. Rev. E* **93**, 032215 (2016)
42. Wang, L., Zhu, Y.J., Wang, Z.Q., Xu, T., Qi, F.H., Xue, Y.S.: Asymmetric Rogue waves, breather-to-soliton conversion, and nonlinear wave interactions in the Hirota–Maxwell–Bloch system. *J. Phys. Soc. Jpn.* **85**, 024001 (2016)
43. Wang, L., Li, S., Qi, F.H.: Breather-to-soliton and rogue wave-to-soliton transitions in a resonant erbium-doped fiber system with higher-order effects. *Nonlinear Dyn.* **85**, 389 (2016)
44. Wang, L., Zhang, J.H., Wang, Z.Q., Liu, C., Li, M., Qi, F.H., Guo, R.: Breather-to-soliton transitions, nonlinear wave interactions, and modulational instability in a higher-order generalized nonlinear Schrödinger equation. *Phys. Rev. E* **93**, 012214 (2016)
45. Wang, L., Zhang, J.H., Liu, C., Li, M., Qi, F.H.: Breather transition dynamics, Peregrine combs and walls, and modulation instability in a variable-coefficient nonlinear Schrödinger equation with higher-order effects. *Phys. Rev. E* **93**, 062217 (2016)
46. Wang, L., Wang, Z.Q., Zhang, J.H., Qi, F.H., Li, M.: Stationary nonlinear waves, superposition modes and modulational instability characteristics in the AB system. *Nonlinear Dyn.* **86**, 185 (2016)
47. Liu, C., Yang, Z.Y., Zhao, L.C., Yang, W.L.: Transition, coexistence, and interaction of vector localized waves arising from higher-order effects. *Ann. Phys.* **362**, 130 (2015)
48. Ren, Y., Yang, Z.Y., Liu, C., Yang, W.L.: Different types of nonlinear localized and periodic waves in an erbium-doped fiber system. *Phys. Lett. A* **379**, 2991 (2015)

49. Zhang, J.H., Wang, L., Liu, C.: Superregular breathers, characteristics of nonlinear stage of modulation instability induced by higher-order effects. *Proc. R. Soc. A* **473**, 20160681 (2017)
50. Chowdury, A., Ankiewicz, A., Akhmediev, N.: Moving breathers and breather-to-soliton conversions for the Hirota equation. *Proc. R. Soc. A* **471**, 20150130 (2015)
51. Chowdury, A., Kedziora, D.J., Ankiewicz, A., Akhmediev, N.: Breather-to-soliton conversions described by the quintic equation of the nonlinear Schrödinger hierarchy. *Phys. Rev. E* **91**, 032928 (2015)
52. Zakharov, V.E., Gelash, A.A.: Nonlinear stage of modulation instability. *Phys. Rev. Lett.* **111**, 054101 (2013)
53. Yang, J.W., Gao, Y.T., Wang, Q.M., Su, C.Q., Feng, Y.J., Yu, X.: Bilinear forms and soliton solutions for a fourth-order variable-coefficient nonlinear Schrödinger equation in an inhomogeneous Heisenberg ferromagnetic spin chain or an alpha helical protein. *Phys. B* **481**, 148 (2016)
54. Yang, J.W., Gao, Y.T., Su, C.Q., Wang, Q.M., Lan, Z.Z.: Breathers and rogue waves in a Heisenberg ferromagnetic spin chain or an alpha helical protein. *Commun. Nonlinear Sci. Numer. Simul.* **48**, 340 (2017)
55. Xie, X.Y., Tian, B., Chai, J., Wu, X.Y., Jiang, Y.: Dark soliton collisions for a fourth-order variable-coefficient nonlinear Schrödinger equation in an inhomogeneous Heisenberg ferromagnetic spin chain or alpha helical protein. *Nonlinear Dyn.* **86**, 131 (2016)
56. Su, C.Q., Qin, N., Li, J.G.: Conservation laws, nonautonomous breathers and rogue waves for a higher-order nonlinear Schrödinger equation in the inhomogeneous optical fiber. *Superlattices Microstruct.* **100**, 381 (2016)
57. Ankiewicz, A., Soto-Crespo, J.M., Akhmediev, N.: Rogue waves and rational solutions of the Hirota equation. *Phys. Rev. E* **81**, 046602 (2010)
58. Tao, Y.S., He, J.S.: Multisolitons, breathers, and rogue waves for the Hirota equation generated by the Darboux transformation. *Phys. Rev. E* **85**, 026601 (2012)
59. Chowdury, A., Kedziora, D.J., Ankiewicz, A., Akhmediev, N.: Breather solutions of the integrable quintic nonlinear Schrödinger equation and their interactions. *Phys. Rev. E* **91**, 022919 (2015)
60. Yang, R.C., Li, L., Hao, R.Y., Li, Z.H., Zhou, G.S.: Combined solitary wave solutions for the inhomogeneous higher-order nonlinear Schrödinger equation. *Phys. Rev. E* **71**, 036616 (2005)
61. Yin, H.M., Tian, B., Zhen, H.L., Chai, J., Liu, L., Sun, Y.: Solitons, bilinear Bäcklund transformations and conservation laws for a (2+1)-dimensional Bogoyavlenskii–Kadomtsev–Petviashvili equation in a fluid, plasma or ferromagnetic thin film. *J. Mod. Opt.* **64**, 725 (2012)
62. Sabry, R., Moslem, W.M., Shukla, P.K.: Amplitude modulation of hydromagnetic waves and associated rogue waves in magnetoplasmas. *Phys. Rev. E* **86**, 036408 (2012)